Magn Reson Mater Phy
DOI 10.1007/s10334-010-0201-3

RESEARCH ARTICLE

Distribution and fibre field similarity mapping of the human anterior commissure fibres by diffusion tensor imaging

Markand Dipankumar Patel · Nicolas Toussaint · Geoffrey David Charles-Edwards · Jean-Pierre Lin · Philip G. Batchelor

Received: 2 August 2009 / Revised: 10 January 2010 / Accepted: 1 February 2010

Abstract
Object The anterior commissure is a critical interhemispheric pathway in animals, yet its connections in humans are not clearly understood. Its distribution has shown to vary greatly between species, and it is thought that in humans it may convey axons from a larger territory than previously thought. The aim was to use an anatomical mapping tool to look at the anterior commissure fibres and to compare the distribution findings with published anatomical understanding.
Materials and methods Two different diffusion-weighted imaging data sets were acquired from eight healthy subjects using a 3 Tesla MR scanner with 32 gradient directions. Diffusion tensor imaging tractography was performed, and the anterior commissure fibres were selected using three-dimensional regions of interest. Distribution of the fibres was observed by means of registration with T2-weighted images. The fibre field similarity maps were produced for five of the eight subjects by comparing each subject's fibres to the combined map of the five data sets.
Results Fibres were shown to lead into the temporal lobe and towards the orbitofrontal cortex in the majority of subjects. Fibres were also distributed to the parietal or occipital lobes in all five subjects in whom the anterior commissure was large enough for interhemispheric fibres to be tracked through. The fibre field similarity maps highlighted areas where the local distances of fibre tracts were displayed for each subject compared to the combined bundle map.
Conclusion The anterior commissure may play a more important role in interhemispheric communication than currently presumed by conveying axons from a wider territory, and the fibre field similarity maps give a novel approach to quantifying and visualising characteristics of fibre tracts.

Keywords Anterior commissure · DTI · Local distance function · Corpus callosum

Abbreviations

AC	Anterior commissure
CC	Corpus callosum
DTI	Diffusion tensor imaging
DWI	Diffusion-weighted imaging
STIR	Short TI inversion recovery

Introduction

The cerebral hemispheres are interconnected by the corpus callosum (CC) and the anterior, posterior and hippocampal commissures. The largest of these connections is the CC spanning across the length of the cerebral hemispheres, providing the majority of interhemispheric information transfer. In those who have complete sections of the CC, it has been shown that motor, language, cognitive and behavioural

M. D. Patel (✉) · N. Toussaint · G. D. Charles-Edwards · P. G. Batchelor
Division of Imaging Sciences, King's College London, London, SE1 7EH, UK
e-mail: markand.patel@kcl.ac.uk; markandpatel@gmail.com

G. D. Charles-Edwards
Medical Physics, Guy's & St Thomas' NHS Foundation Trust, London, UK

J.-P. Lin
Department of Paediatric Neurology, Guy's & St Thomas' NHS Foundation Trust, London, UK
e-mail: Jean-Pierre.Lin@gstt.nhs.uk

Published online: 13 March 2010

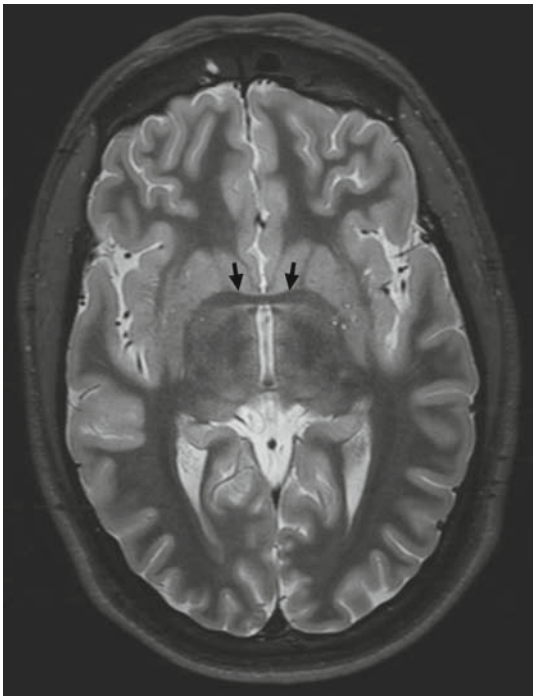

Fig. 1 Inversion recovery sequence image of an axial slice at the level of the anterior commissure, highlighting its connection between both hemispheres

functions can remain unaffected [1,2]. This suggests alternative routes play a part, and in particular the anterior commissure (AC), as seen in Fig. 1, has been shown to provide many interhemispheric routes for information [3]. Investigating these connections of the AC may be important in the understanding of epileptic spread between the hemispheres, since both the CC and the hippocampal commissure have been shown to be critical in the contralateral spread of electrical potentials [1]. Limiting seizure spread in those with uncontrolled epilepsy is possible by sectioning the commissural fibres and has shown to prevent an unconscious state during seizures [1,4]. It is common to leave the AC intact during surgical procedures for epilepsy, and it may be possible for epileptic potentials to travel through this pathway, inducing bilateral spread [1].

The mid-sagittal cross-sectional area of the AC has been shown to be 1% of the CC area, and variations in the area are thought to represent the distribution of interhemispheric communication [5]. Hypertrophy of the AC especially in congenital agenesis of the CC may be due to re-routing of some neuronal axons for better functional compensation [6,7]. An increase in the total number of axons passing through the AC without hypertrophy has also been observed in acallosal mice, suggesting it can be used as an alternative pathway for information transfer [8].

Distribution of the AC to various parts of the brain in animals has been shown to vary greatly between species [9,10]. For species that do not possess a CC, the AC is the largest and most critical interhemispheric pathway, carrying the CC-related functions [7,10–13]. Relatively less work has looked at the human AC, and until recently it was presumed that the commissure has connections similar to non-human primates, but is now thought to convey axons from a much larger territory [14].

The AC in humans is classically divided into two distinct tracts, the anterior and posterior limbs. The anterior limb connects to the olfactory bulbs, their nuclei and the inferior-posterior orbital gyri and is thought to be a minor component of the AC fibre tracts [14,15]. It is thought that phylogenetically as the functions of the olfactory complex regress, connections of the AC appear to shift to neocortical regions in the temporal lobes, to which the corpus callosum does not project [10,16,17].

The posterior limb travels within the basal part of the striatum and into the temporal cortex towards the amygdala [18], temporal pole [19], parahippocampal, inferior temporal and fusiform gyri [14,20–22]. Additional afferents from the occipital cortex, precentral gyrus and central fissure have been described through the posterior limb [14].

Studies in humans looking at the fibres passing through the AC have mostly involved dissections of the brain, followed by staining and tracing. However, with recent advances in MRI neuroimaging techniques tractography from DTI data enables the construction of pathways of high water diffusion that are associated with white matter fibre tracts in the brain, thereby allowing visualisation and investigation of connections between different brain regions, in vivo and noninvasively. This can be used to better comprehend the fibre connections through the AC.

DTI uses a set of diffusion-weighted MR images acquired in at least six directions to enable estimation of the diffusion tensor in each voxel. Tractography algorithms, such as streamlines, can then display the path of the principle direction of diffusion in anisotropic tissue until termination in areas of low anisotropy. Large anisotropic diffusion is observed in white matter, where molecular motion is greater parallel to the myelinated axonal fibres rather than perpendicular to them [23]. Fibres reconstructed, therefore, represent paths of the most probable direction of molecular diffusion, hence along the axonal fibres.

DTI has shown distribution of the AC fibres to the amygdala and temporal pole as well as the ventrolateral temporo-occipital cortex [24–26], supporting Di Virgilio et al. [14] who illustrated through dissection that the AC receives axons from the inferior occipital cortex in man and that these connections are not present in macaque [27].

This study aims to use DTI-based tractography with an anatomical mapping tool to look at the AC fibres and to compare the distribution findings with published anatomical understanding.

Materials and methods

Subjects and image acquisition

Data were acquired from eight healthy subjects using a Philips Achieva 3T MRI system with an eight-channel head coil. Two DTI data sets were acquired from each subject with b-values of $0, 1{,}000\,\mathrm{s/mm^2}$ and $0, 1{,}500\,\mathrm{s/mm^2}$, respectively. Echoplanar imaging with a simple Stejskal–Tanner sequence was used with a TR/TE of 10,313/55 and 18,750/50.5 ms, respectively, with acquisition times of 7 min 38 s and 12 min 58 s. A lower TE was used with a b-value of $1{,}500\,\mathrm{s/mm^2}$ to compensate for the reduced signal-to-noise ratio at this higher diffusion weighting. Other acquisition parameters were $2 \times 2 \times 2$ mm voxels, 60 slices, FOV = 224 mm, matrix size = 112×112, partial Fourier = 0.678, SENSE factor = 2 and 32 diffusion-encoding directions. This was repeated on a separate occasion with three of the subjects using identical acquisition parameters to obtain data for assessing reproducibility.

Conventional T2-weighted volumes were acquired for anatomical localisation of the fibre tracts in each subject with a TR/TE of 3,000/80 ms and voxel size of $0.449 \times 0.449 \times 4$ mm. STIR (short TI inversion recovery) images with a TR/TE/TI of 4,811/9.1/200 ms, voxel size of $0.449 \times 0.449 \times 2$ mm and slice spacing of 2 mm were also acquired in the sagittal plane from each subject to produce images for optimum visualisation of the AC for size measurements and region of interest selection.

Data processing

The STIR data sets were registered with the $b = 0$ volume from the DTI data using rigid manual landmark-based methods in MedINRIA ImageFusion to produce transformation matrices. Points that were clearly visible on both images were selected, including along the border of the AC and edges of the globus pallidus and lateral ventricles. Tensor estimation and fibre tracking was performed for each of the data sets in MedINRIA DTI Track [28] using the standard streamline approach for tractography [29,30], in which every voxel of the data set was used as a seed point. The algorithm introduced a stabilisation "advection" vector to minimise fluctuations introduced by low anisotropy regions (especially planar tensors) [31]. The parameter controlling the smoothness of the tracking process is a factor between 0 and 1. A weighting factor of 0.20 was chosen as advised by Weinstein et al. [31] which affects "how much the propagation should be encouraged to puncture through planar tensor areas". In this framework, this parameter replaces an angle threshold used in the basic streamline approach. The anisotropy threshold was set to 0.3. All fibres were generated prior to the region of interest selection, using every valid voxel of the data set, where every voxel containing a positive tensor with a fractional anisotropy greater than or equal to 0.3 as seed point. These fibre fields were then transformed using the previously acquired matrices, and the STIR images were used to produce two three-dimensional regions of interest either side of the AC, by manually drawing around the AC on up to three sagittal slices either side of the midline. After this, only fibres passing through both AC regions of interest from one hemisphere to the other were retained.

In total, there were AC fibre tracts from 22 unique data sets. Six of these data sets from three subjects were unusable as no interhemispheric fibre connections through the AC were produced on tractography. The AC fibre data for each of the remaining five subjects were then manually registered with each other using rigid landmark-based registration to ensure the AC was not translated across subjects. A Procrustes algorithm is used by MedINRIA ImageFusion to perform this registration [32]. Initially, several landmarks distant from the AC were used, such as the tips of the lateral ventricles, edges of the globus pallidus and vertex of the brain for correcting obvious misorientation. Landmarks were then focussed around the AC for more subtle alignments, including the most inferior-posterior point in the AC as well as recognisable neuroanatomical features such as the inferior border of septum pellucidum, the anterior border of the fornix and the inferior portion of the corpus callosum. It was then possible to produce a combined map of the total AC fibres across the five subjects.

The T2-weighted volumes were also registered with the $b = 0$ volume using rigid manual landmark-based methods. The AC fibre bundles were visualised on the T2-weighted volumes, as seen in Fig. 2, along with the STIR volumes to assess distribution of the fibres.

Intra-subject reproducibility

Two different diffusion weightings were used in all subjects and repeat scans acquired from three of the subjects, in order to assess reproducibility of the fibres tracked through the AC. A b-value of $1{,}000\,\mathrm{s/mm^2}$ was used as it is found to be the most common and clinically useful diffusion weighting. A larger b-value of $1{,}500\,\mathrm{s/mm^2}$ was also used to assess whether it is consistent with the findings at $1{,}000\,\mathrm{s/mm^2}$. In each of the fibre data sets, the number of fibres passing through the AC from one hemisphere to the other were counted, and this was compared to the mid-sagittal cross-sectional area of the AC in that subject.

The AC cross-sectional area was calculated from the sagittal section STIR images by measuring the AC maximum height and its perpendicular width on the Philips scanner image viewing software. This was in turn used to calculate the ellipsoid area of the AC. The CC cross-sectional area

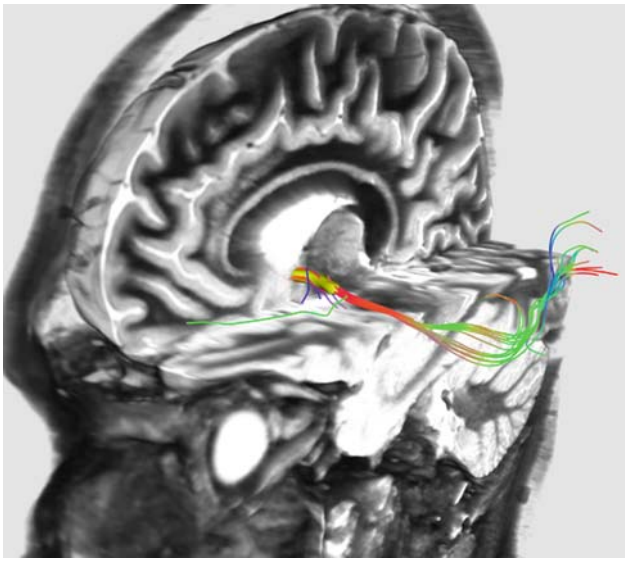

Fig. 2 Image showing the anterior commissure fibres from a single subject projected onto the three-dimensional T2-weighted volume, for assessing distribution of the tracts

was also calculated in the midline sagittal plane, using Sante DICOM viewer [33]. Being a larger structure, a region of interest could be drawn around the CC on the mid-sagittal STIR images, and its area was automatically calculated.

Fibre field similarity measure

Each subject's data set was extracted from the combined map of five subjects and then compared with the remaining pooled four sets of data, hence using the 'leave one out method' to calculate the fibre field similarity.

To locally identify dissimilarities between bundles L_1 and L_2, a local distance function denoted as $d^2(L_1, L_2)$ was used. The fibre field resulting from the DTI acquisition and fibre tracking consisted of a set of three-dimensional curves following the primary eigenvector of the diffusion tensors. The similarity measure between two fibre fields was computed by embedding curves in the space of currents. Curves can be considered as geometrical primitives that can be modelled as *currents* [34,35]. The idea was to characterise shapes via vector fields that are used to probe them. A current is the flux of a vector field through the geometric shape. In the case of a curve L, a current is the path integral of any vector field ω through the curve:

$$\forall \omega \in W, L : \omega \rightarrow \int_L \langle \omega\,(l)\,|\tau\,(l)\rangle_{IR^3}\,\mathrm{d}l \tag{1}$$

where $\tau(l)$ is the unit tangent, and W is the 'test' space where the vector field is defined. As described by Durrleman et al. [35], the test space was constrained to the space of smooth vector fields ω, following $|\omega| < 1$. Considering two sets of curves containing N_1 and N_2 points, this framework allows the definition of a distance between the two sets as an inner product in the Hilbert space as in Durrleman et al. [35], giving

$$\begin{aligned} d^2\left(L_1, L_2\right) &= |L_1 - L_2|^2 = \left\langle L_1 - L_2,\ L_1 - L_2 \right\rangle_W \\ &= \sum_{i=1}^{i<N_1} \sum_{j=1}^{i<N_2} (\tau_i)^t . \mathrm{e}^{-\|p_i - p_j\|/\lambda^2} . \left(\tau_j\right)^t \end{aligned} \tag{2}$$

where τ_i and τ_j corresponded to unit tangent vectors at positions p_i and p_j. The exponential term corresponds to the Gaussian kernel of variance λ and captures local spatial distance between curves. The dot product between the tangents captures the difference in orientation between curves. This distance has the property to not assume any point correspondence between points. However, this similarity measure between curves (or sets of curves) gives a global distance between two fibre fields.

Additionally to the framework by Glaunes et al. [34] and Durrleman et al. [35], the distance definition was extended to a local one. Considering a set of curves L, a local version L' can be defined by convolution of L with a Gaussian kernel of variance σ centred in p:

$$L'(p) = L * \mathrm{e}^{-\|x-p\|/\sigma^2} \tag{3}$$

Thanks to this localisation, the influence of the set of curves was constrained to those close to the point where the distance was measured. It is then possible to define the local distance in p between two sets of curves L_1 and L_2 by:

$$d^2\left(L_1, L_2\right)(p) = \left\langle L_1'(p) - L_2'(p),\ L_1'(p) - L_2'(p) \right\rangle_W \tag{4}$$

This enabled visualisation of the local distance difference of a particular bundle to the rest of the population.

Results

Reproducibility of tractography

The fibres tracked through the AC from the different diffusion-weighted and repeat acquisitions are shown in Fig. 3 for the five subjects. Although the distribution of the major fibre bundles appear similar when scans are repeated, the number of fibres does vary, especially when the diffusion weighting is increased.

The number of fibres passing through the AC, its cross-sectional area in the midline and its relation to the CC size are shown in Table 1. These results are plotted on a graph in Fig. 4, omitting the subjects in whom tractography was unsuccessful. Using linear regression, a good correlation was found between the AC mid-sagittal cross-sectional area

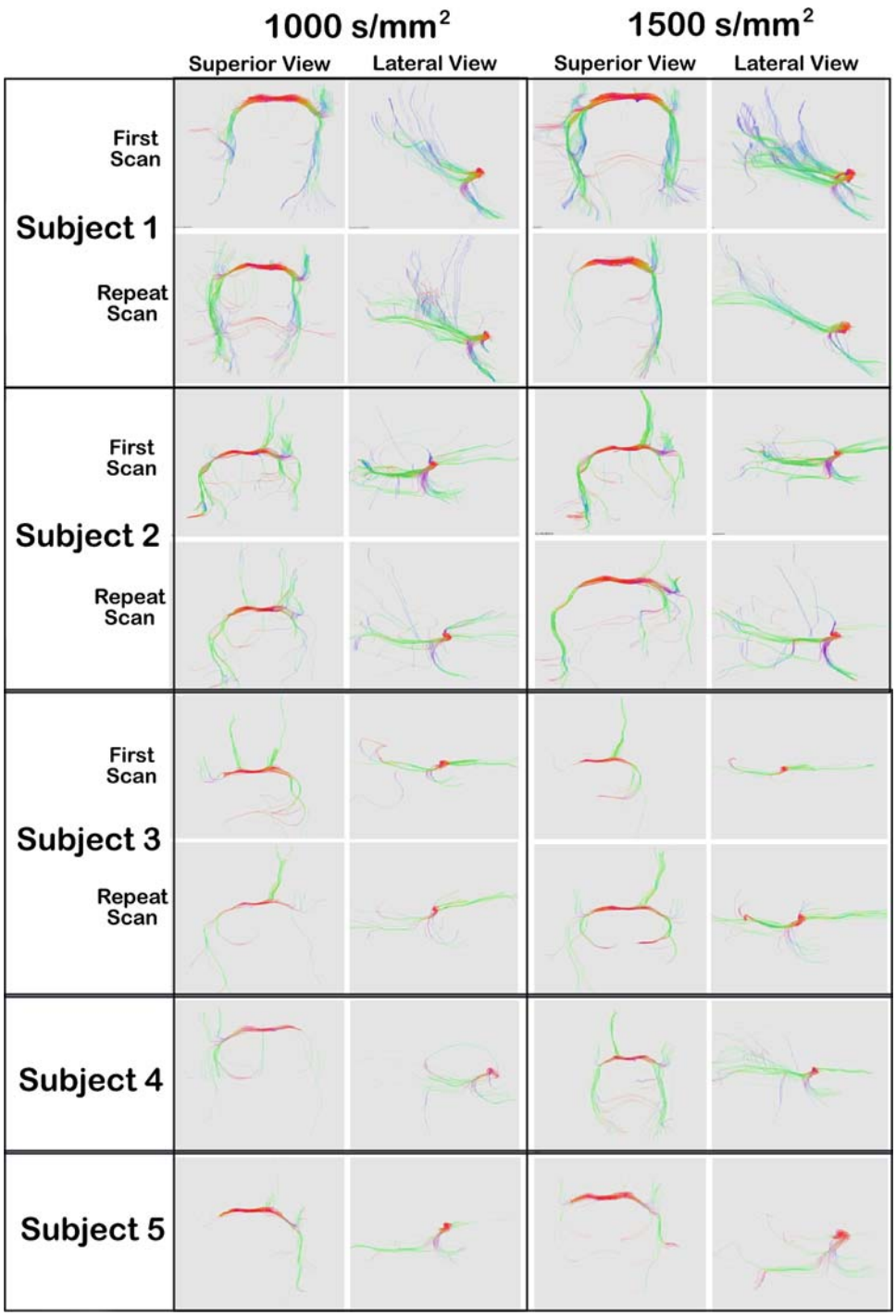

Fig. 3 Fibres tracked through the AC in the five subjects, with differences between diffusion weightings and the first and repeat scans. The two views shown are the superior and right lateral views of the fibres

and the number of fibres passing through it at a *b*-value of 1,000 s/mm^2, although there was greater variation of fibre numbers at a *b*-value of 1,500 s/mm^2.

Distribution and fibre field similarity

Fibre tracking revealed large differences in the distribution of AC fibres across subjects. *Tractography from subject 1*, as seen in Fig. 3, showed a large proportion of fibres in the posterior limb of the AC travelling bilaterally above the hippocampus into the parietal lobe, especially into the inferior parietal lobule where the majority terminated. Another bundle carried on further to the superior parietal lobule and postcentral gyrus, with a smaller bundle to the precentral gyrus. The other portion of the posterior limb entered the temporal lobe towards the amygdala, but much more so on the right

Table 1 Anterior commissure and corpus callosum mid-sagittal cross-sectional areas measured from the inversion recovery images, with size ratios and number of fibres tracked through the anterior commissure for the various acquisitions

Subject	AC Area (mm^2)	CC Area (cm^2)	AC:CC Size ratio	Number of fibres through AC			
				1,000 s/mm^2		1,500 s/mm^2	
				First scan	Repeat scan	First scan	Repeat scan
1	11.79	6.39	1:54	253	190	351	162
2	9.32	6.85	1:74	156	85	168	93
3	5.93	7.56	1:128	67	34	57	60
4	5.37	7.91	1:147	39	–	114	–
5	8.16	6.58	1:80	118	–	118	–
6	1.98	5.52	1:278	0	–	0	–
7	1.90	5.69	1:299	0	–	0	–
8	7.04	7.47	1:106	0	–	0	–

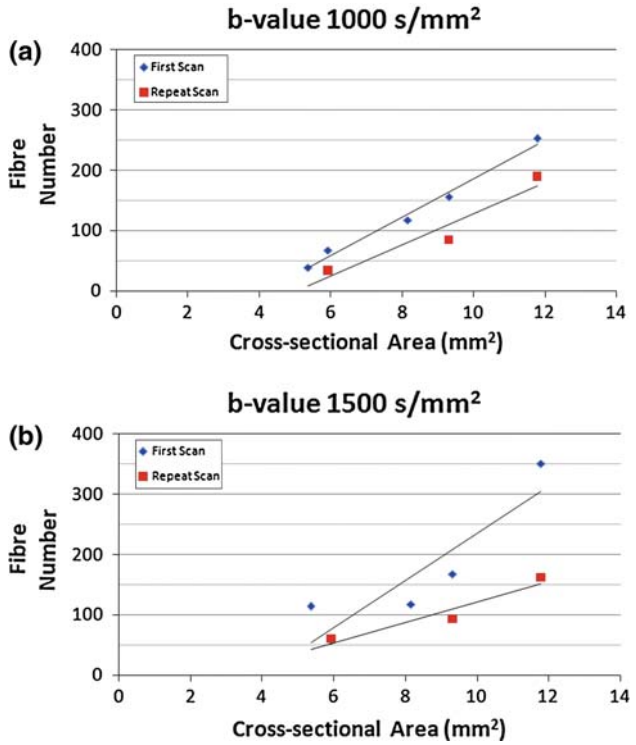

Fig. 4 Graphs showing the relationship between the anterior commissure mid-sagittal cross-sectional area and the number of fibres tracked through it for **a** the acquisitions at 1,000 s/mm^2 and **b** acquisitions at 1,500 s/mm^2

than left side. There was no anterior limb of the AC visible. Although there was a wide distribution of fibres from the AC through the posterior limb, the fibre field similarity maps showed a large Hilbert distance projected onto the parietal lobe fibres and fibres crossing the corpus callosum and a small Hilbert distance in the main trunk of the posterior limbs, as shown in Fig. 5.

Tractography from subject 2 showed posterior limb fibres travelling into the occipital lobe bilaterally, with a larger number on the left. There were also temporal lobe fibres through this limb, with a large number on the right. The anterior limb contained fibres towards the orbitofrontal cortex bilaterally. Fibre field similarity maps showed a large Hilbert distance in the left temporal lobe, where there were fewer fibres than on the right and a relatively small Hilbert distance in the anterior limbs.

Tractography from subject 3 showed a very small number of fibres compared to the other subjects, although the majority of these made up the anterior limb bilaterally towards the orbitofrontal cortex. The posterior limb showed small numbers of fibres into the occipital lobe and the temporal lobe bilaterally. Fibre field similarity maps showed a large Hilbert distance in the occipital lobes and a relatively small Hilbert distance in the body of the AC.

Tractography from subject 4 showed bundles travelling into the parietal and temporal lobes bilaterally. The anterior limb fibres towards the orbitofrontal cortex were also present on the right. Fibre field similarity maps showed a large Hilbert distance in the anterior limb and body of the AC.

Tractography from subject 5 showed the posterior limb fibres to the occipital lobe and temporal lobe mostly on the right, as well as the anterior limb fibres for a short distance bilaterally towards the orbitofrontal cortex. Fibre field similarity maps showed a large Hilbert distance in the right posterior limb and relatively low Hilbert distance in the body of the AC.

Discussion

Using tractography the fibres passing through the AC for five of the subjects were isolated, fibre distributions were determined, and the fibre field similarity for each subject was calculated. The distribution of fibres through the AC was shown

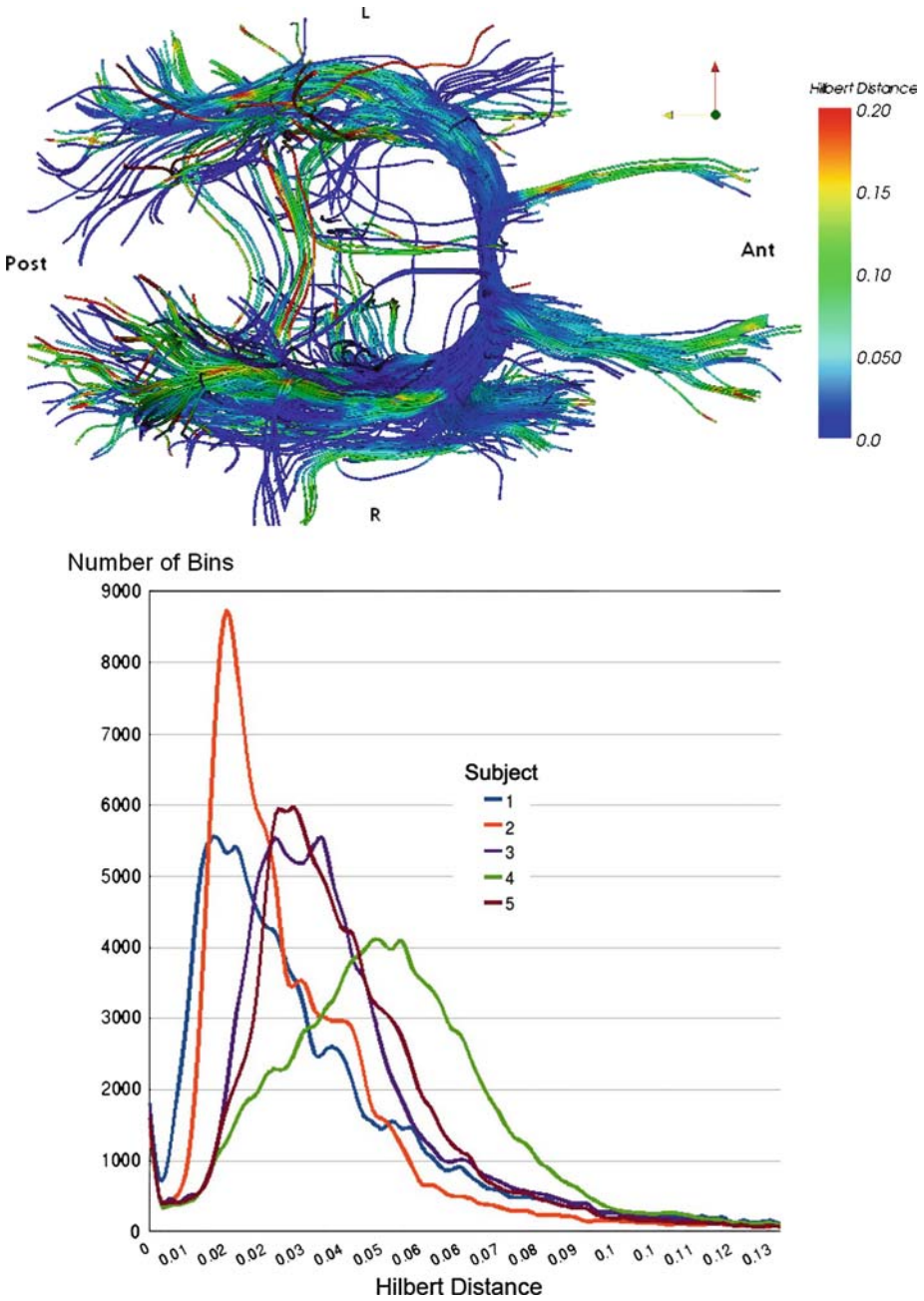

Fig. 5 Image showing the fibre field similarity map produced for subject 1 from a superior view of the brain. The fibres are colour labelled with the Hilbert distance, a measure of the local distance between each subjects' fibre tracts and the combined map. The histogram represents the Hilbert distances for each of the subjects 1–5

in all subjects to pass via the posterior limb to the temporal lobe and either the occipital or parietal lobes. The temporal lobe connections of the AC fibres to the amygdala and temporal pole were seen in the majority of subjects, as described in the literature [18–22]. The parietal lobe fibres were seen in two of the five subjects, and occipital lobe fibres in the remaining three subjects. This is in line with results from the dissection study by Di Virgilio et al. [14] which showed connections to the occipital cortex, central fissure and precentral gyrus, as well as DTI studies showing fibres from the AC extending to the ventrolateral occipital cortex [24–26].

The anterior limb which extends towards the orbitofrontal cortex after passing through the AC was visible to some extent bilaterally in four of the five volunteers and has been described in the literature [15]. This data is consistent with observations from Di Virgilio et al. [14], suggesting that axons to the AC may be conveyed from a larger territory than previously proposed, specifically from parts of the occipital cortex and various parts of the parietal lobe. This may be due to connections of the AC shifting phylogenetically to neocortical areas where the corpus callosum does not project [10,16,17].

As shown in Table 1, the CC area varied between 54 and 299 times the AC cross-sectional area; hence, the AC being 0.3–1.8% of the CC area. This supports the study by Foxman et al. [5] that the AC area is about 1% of the CC

cross-sectional area. It has been suggested that a larger commissural area would have more nerve fibres crossing between the hemispheres, and consequently those cognitive functions that rely on only one hemisphere are more likely to be shared, and therefore less dependent on that one hemisphere [36].

The correlation between AC fibre number and cross-sectional area was as expected and shown not be a result of postprocessing techniques. A *b*-value of 0, 1,000 s/mm^2 is typically the standard value used for clinical DWI [37]. As the *b*-value increases, the signal intensity decreases as the contributions of T1 and T2 weighting decrease, leading to a reduced signal-to-noise ratio as DWI signals are closer to the background noise level [38], but having an increased diffusion sensitivity [39,40]. This may explain why the repeat scans with a *b*-value of 1,000 s/mm^2 were more consistent than at 1,500 s/mm^2. Due to the higher level of background noise, there was much greater variation when scans were repeated, and consequently the number of fibres passing through the AC also varied considerably. At a *b*-value of 1,500 s/mm^2, there will have been greater diffusion sensitivity and consequently better estimation of fibre direction where nerve fibres cross, and so it may suggest the general increase in fibre numbers when compared with a *b*-value of 1,000 s/mm^2.

One observation noted was that out of the eight subjects, there were five in which results were obtained, and the remaining three subjects' data sets could not be used due to a lack of AC fibres passing from one hemisphere to the other. As seen in Table 1, two of those subjects had AC cross-sectional areas of below 2 mm^2, which were considerably smaller than the subjects in which tractography through the AC was successful. The last subject had an AC cross-sectional area of 7.04 mm^2 which is in the middle of the successful range of areas, yet there were still no fibres produced on tractography. Fibres were produced in the structures surrounding the AC, such as the fornix, yet none passed through the AC itself.

The fibre field similarity measure provided a novel approach to calculation and visualisation of the distance between bundles for a particular region of interest, using fibre data between subjects. This technique can aid in the segmentation of white matter bundles within the brain, by identifying the extent to which fibres are anatomically distant from the population map. Fibres that appear to have a large Hilbert distance may be classed as outlying fibres which do not lie close to the overall population fibre bundles. This along with other fibre characteristics such as curvature and torsion appears to have applications for looking at normal versus abnormal fibre tracts for example in the presence of a tumour [41].

Limitations

Although the fibre field similarity measures and maps are very useful, there were limitations in this study as comparing across subjects meant that any large anatomical differences between the subjects would affect the fibre field similarity calculations, causing a larger Hilbert distance to be displayed if for example the brain size was significantly different to the population.

There are also several limitations when using DTI to look specifically at fibres through the AC. Since microscopic information is averaged over the volume of the voxel, in areas where anatomically large fibre tracts come close to smaller fibre bundles, a proportion of fibres closest to the larger tracts appear to follow incongruent paths indicative of falsely reconstructed fibre paths. This could be the case with the posterior limb of the AC, as anatomically the axons pass posteriorly before turning anteriorly into the temporal lobe. Lying close to this bundle is the inferior longitudinal fasciculus and fronto-occipital fasciculus, which transverse the entire length of the brain and enter the temporal and occipital lobes, respectively [42]. Since these pass fairly close to the AC axons, it may be possible that with DTI several fasciculi fibres are picked up erroneously as AC fibres to the occipital lobe. Anatomical differences of crossing white matter tracts between subjects may explain the inter-subject variation of AC distribution as seen in Fig. 3, as it causes premature termination of the streamlines at various points along the AC fibres. Intra-subject comparisons of the AC fibres shows fairly similar tracts, although these differences may be explained by changes in the magnetic field inhomogeneities due to the time difference between the first and repeat scans.

Ways to overcome the effects due to crossing fibres would be to first improve the imaging resolution, for example by using fast spin-echo DTI which allows sub-millimetre voxel sizes, and also means that multiple voxels can characterise the smaller anterior commissures in subjects [43]. Secondly, other methods apart from conventional streamline tractography can be used, such as high angular resolution diffusion imaging (HARDI) and Q-ball imaging (QBI), which allow better reconstruction in areas with crossing fibres [44–46]. It is at present difficult to trust the connectivity maps of the AC, but these methods may help define the normal anatomy of the AC which is still under question from past dissection studies and recent DTI work. They may also help overcome the unsuccessful AC tractography in the last subject from Table 1, where the problem may be related to the angle at which the AC and the fornix are related. The fornix branches off the AC just prior to the AC crossing from one hemisphere to the other. If the angle of the white matter tract is steeper within the AC than the fornix, it may be possible that the fibres reconstructed represent those of only the fornix. Therefore, HARDI and QBI would be more appropriate and allow a more reliable reconstruction of the AC fibre tracts, hence giving a better understanding of the posterior limb connections of the AC, and how the AC cross-sectional area relates to distribution.

Conclusion

This DTI study has shown that the AC may play a more important role in interhemispheric communication than currently presumed by conveying axons from a wider territory, specifically from the occipital cortex and parietal lobes. This may be clinically relevant in the spread of electrical potentials from one hemisphere to the other in patients with epilepsy. The study has also looked at the reproducibility of the AC fibre tracts using DTI, confirming the previously recognised temporal and orbitofrontal projections, and given a novel approach to quantifying and visualising characteristics of these fibre tracts through fibre field similarity measures and maps. However, further work with improved technical and processing methods is required to more accurately characterise these AC fibres and its normal anatomy.

References

1. Spencer SS (1988) Corpus callosum section and other disconnection procedures for medically intractable epilepsy. Epilepsia 29(s2):S85–S99
2. Berlucchi G, Aglioti S, Marzi CA, Tassinari G (1995) Corpus callosum and simple visuomotor integration. Neuropsychologia 33(8):923–936
3. Risse GL, LeDoux J, Springer SP, Wilson DH, Gazzaniga MS (1978) The anterior commissure in man: functional variation in a multisensory system. Neuropsychologia 16(1):23–31
4. Amacher AL (1976) Midline commissurotomy for the treatment of some cases of intractable epilepsy. Preliminary report. Childs Brain 2(1):54–58
5. Foxman BT, Oppenheim J, Petito CK, Gazzaniga MS (1986) Proportional anterior commissure area in humans and monkeys. Neurology 36(11):1513–1517
6. Fischer M, Ryan SB, Dobyns WB (1992) Mechanisms of interhemispheric transfer and patterns of cognitive function in acallosal patients of normal intelligence. Arch Neurol 49(3):271–277
7. Bamiou DE, Sisodiya S, Musiek FE, Luxon LM (2007) The role of the interhemispheric pathway in hearing. Brain Res Rev 56(1):170–182
8. Livy DJ, Schalomon PM, Roy M, Zacharias MC, Pimenta J, Lent R, Wahlsten D (1997) Increased axon number in the anterior commissure of mice lacking a corpus callosum. Exp Neurol 146(2):491–501
9. Horel JA, Stelzner DJ (1981) Neocortical projections of the rat anterior commissure. Brain Res 220(1):1–12
10. Pandya DN, Karol EA, Lele PP (1973) The distribution of the anterior commissure in the squirrel monkey. Brain Res 49(1):177–180
11. Ehrlich D, Mills D (1985) Myelogenesis and estimation of the number of axons in the anterior commissure of the chick (Gallus gallus). Cell Tissue Res 239(3):661–666
12. Glickstein M (2009) Paradoxical inter-hemispheric transfer after section of the cerebral commissures. Exp Brain Res 192(3):425–429
13. Ashwell KW, Marotte LR, Li L, Waite PM (1996) Anterior commissure of the wallaby (Macropus eugenii): adult morphology and development. J Comp Neurol 366(3):478–494
14. Di Virgilio G, Clarke S, Pizzolato G, Schaffner T (1999) Cortical regions contributing to the anterior commissure in man. Exp Brain Res 124(1):1–7
15. Kiernan JA, Barr ML (1998) Barr's the human nervous system: an anatomical viewpoint. Lippincott-Raven, New York
16. Fox CA, Fisher RR (1948) The distribution of the anterior commissure in the monkey, *Macaca mulatta*. J Comp Neurol 89(3):245–277
17. Karol EA, Pandya DN (1971) The distribution of the corpus callosum in the Rhesus monkey. Brain 94(3):471–486
18. Turner BH, Mishkin M, Knapp ME (1979) Distribution of the anterior commissure to the amygdaloid complex in the monkey. Brain Res 162(2):331–337
19. Demeter S, Rosene DL, Van Hoesen GW (1990) Fields of origin and pathways of the interhemispheric commissures in the temporal lobe of macaques. J Comp Neurol 302(1):29–53
20. Jacobson S, Marcus EM (2008) Neuroanatomy for the neuroscientist. Springer, New York
21. Johnston JM, Vaishnavi SN, Smyth MD, Zhang D, He BJ, Zempel JM, Shimony JS, Snyder AZ, Raichle ME (2008) Loss of resting interhemispheric functional connectivity after complete section of the corpus callosum. J Neurosci 28(25):6453–6458
22. Demeter S, Rosene DL, Van Hoesen GW (1985) Interhemispheric pathways of the hippocampal formation, presubiculum, and entorhinal and posterior parahippocampal cortices in the rhesus monkey: the structure and organization of the hippocampal commissures. J Comp Neurol 233(1):30–47
23. Le Bihan D, Mangin JF, Poupon C, Clark CA, Pappata S, Molko N, Chabriat H (2001) Diffusion tensor imaging: concepts and applications. J Magn Reson Imaging 13(4):534–546
24. Jellison BJ, Field AS, Medow J, Lazar M, Salamat MS, Alexander AL (2004) Diffusion tensor imaging of cerebral white matter: a pictorial review of physics, fiber tract anatomy, and tumor imaging patterns. AJNR Am J Neuroradiol 25(3):356–369
25. Catani M, Ffytche DH (2005) The rises and falls of disconnection syndromes. Brain 128(Pt 10):2224–2239
26. Catani M, Howard RJ, Pajevic S, Jones DK (2002) Virtual in vivo interactive dissection of white matter fasciculi in the human brain. Neuroimage 17(1):77–94
27. Rockland KS, Pandya DN (1986) Topography of occipital lobe commissural connections in the rhesus monkey. Brain Res 365(1):174–178
28. Toussaint N, Souplet JC, Fillard P (2007) Medinria: medical image navigation and research tool by INRIA. In: Proceedings of MICCAI'07 workshop on interaction in medical image analysis and visualization. Brisbane, Australia
29. Fillard P, Gerig G (2003) Analysis tool for diffusion tensor MRI. In: Proceedings of MICCAI'03, ser. LNCS vol 2878(2), pp 967–968
30. Xu D, Mori S, Solaiyappan M, van Zijl PCM, Davatzikos C (2002) A framework for callosal fiber distribution analysis. Neuroimage 17(3):1131–1143
31. Weinstein D, Kindlmann G, Lundberg E (1999) Tensorlines: advection-diffusion based propagation through diffusion tensor fields. In: Proceedings of the conference on Visualization '99. San Francisco, California, United States
32. Fitzpatrick J, West J (2001) The distribution of target registration error in rigid-body, point-based registration. IEEE Trans Med Imag 20(9):917–927
33. Escott EJ, Rubinstein D (2003) Free DICOM image viewing and processing software for your desktop computer: what's available and what it can do for you. Radiographics 23(5):1341–1357
34. Glaunes J, Qiu A, Miller M, Younes L (2008) Large deformation diffeomorphic metric curve mapping. Int J Comput Vision 80(3):317–336
35. Durrleman S, Pennec X, Trouve A, Thompson P, Ayache N (2008) Inferring brain variability from diffeomorphic deformations of currents: an integrative approach. Med Image Anal 12(5):626–637
36. Kimura D (1999) Sex and cognition. MIT Press, Cambridge

37. Mukherjee P, Chung SW, Berman JI, Hess CP, Henry RG (2008) Diffusion tensor MR imaging and fiber tractography: technical considerations. AJNR Am J Neuroradiol 29(5):843–852
38. Jones DK, Basser PJ (2004) Squashing peanuts and smashing pumpkins: how noise distorts diffusion-weighted MR data. Magn Reson Med 52(5):979–993
39. Mori S, Zhang J (2006) Principles of diffusion tensor imaging and its applications to basic neuroscience research. Neuron 51(5):527–539
40. Meyer JR, Gutierrez A, Mock B, Hebron D, Prager JM, Gorey MT, Homer D (2000) High-b-value diffusion-weighted MR imaging of suspected brain infarction. AJNR Am J Neuroradiol 21(10):1821–1829
41. Batchelor PG, Calamante F, Tournier J-D, Atkinson D, Hill DLG, Connelly A (2006) Quantification of the shape of fiber tracts. Magn Reson Med 55(4):894–903
42. Catani M, Thiebaut de Schotten M (2008) A diffusion tensor imaging tractography atlas for virtual in vivo dissections. Cortex 44(8):1105–1132
43. Gui M, Peng H, Carew JD, Lesniak MS, Arfanakis K (2008) A tractography comparison between turboprop and spin-echo echo-planar diffusion tensor imaging. Neuroimage 44(4):1451–1462
44. Freidlin RZ, Ozarslan E, Komlosh ME, Chang LC, Koay CG, Jones DK, Basser PJ (2007) Parsimonious model selection for tissue segmentation and classification applications: a study using simulated and experimental DTI data. IEEE Trans Med Imaging 26(11):1576–1584
45. Dong Q, Welsh RC, Chenevert TL, Carlos RC, Maly-Sundgren P, Gomez-Hassan DM, Mukherji SK (2004) Clinical applications of diffusion tensor imaging. J Magn Reson Imaging 19(1):6–1843
46. Alexander AL, Lee JE, Lazar M, Field AS (2007) Diffusion tensor imaging of the brain. Neurotherapeutics 4(3):316–329